https://doi.org/10.5028/jatm.v12.1108 ORIGINAL PAPER

Investigation of Aerodynamic Characteristics of a Wing Model With RGV Winglet

Sivaraj Gopal Krishnan[1], Mohammad Hafifi Ishak[1], Mohammad Azwan Nasirudin[1], Farzad Ismail[1,*]

Krishnan SG https://orcid.org/0000-0003-1660-3407
Ishak MH https://orcid.org/0000-0002-2290-3986
Nasirudin MA https://orcid.org/0000-0001-6490-0831
Ismail F https://orcid.org/0000-0003-4635-0156

How to cite

Krishnan SG; Ishak MH; Nasirudin MA; Ismail F (2020) Investigation of aerodynamic characteristics of a wing model with RGV winglet. J Aerosp Technol Manag, 12, e2020. https://doi.org/10.5028/jatm.v12.1108

ABSTRACT: This work describes the aerodynamic characteristics of an aircraft wing model with a Rüppell's griffon vulture (RGV)-type winglet. A computational fluid dynamics (CFD) study using ANSYS 15.0 was conducted to study the effect of the RGV winglet on a rectangular wing. The NACA 65(3)-218 wing consists of 660 mm span and 121 mm chord length where the aspect ratio is 5.45. Eight different winglet configurations have been studied. Furthermore, the study is extended to study effect of cant angle and different angles of attack (AOA) to the winglet. A comparative study is done on aerodynamic features such as lift coefficient (C_L), drag coefficient (C_D), lift/drag ratio (C_L/C_D) and tip vortices to get the best RGV winglet design. The RGV winglet achieved highest C_L compared to other types of winglets configuration. Based on contour plot analysis, the RGV winglet shows lower vortex formation compared to without winglet. The results show about 15 to 30% reduction in drag coefficient and 5 to 25% increase in lift coefficient by using an RGV winglet.

KEYWORDS: Rüppell's Griffon Vulture; Winglet; Computer Fluid Dynamic; Lift coefficient; Drag coefficient.

INTRODUCTION

One of the primary obstacles limiting the performance of an aircraft is the drag that stems from the vortices shed by an aircraft's wings. The strength of this induced drag is proportional to the spacing and radii of these vortices (Anderson 2004). For a number of years many investigations have been carried out to prove the possible benefits of modifying the wingtip flow.

Tip devices have become a popular technique to increase the aerodynamic performances of lifting wings. The idea is to diffuse the strong vortices released at the wingtip and optimize the span wise lift distribution, while maintaining the additional moments on the wing within certain limits (McCormick 1967). For example, winglets have been used to alter the trailing tip vortex system from an aircraft wing and improve the aircraft performance. Because the vortices shed by the wing are strongest at the tip of the wing, the addition of the wingtip surfaces can reduce and diffuse the strength of these vortices, thus reducing the overall induced drag of the aircraft. The lift-induced drag contributes to approximately 40% of the drag produced by a large transport aircraft (Bushnell 2003). The minimum induced drag for planar wings is achieved for an elliptical lift distribution across the span which produces a constant wing downwash according to Munk's theory (Houghton and Carpenter 2003).

1. Universiti Sains Malaysia - School of Aerospace Engineering - Penang - Malaysia
***Correspondence author:** aefarzad@usm.my
Received: 26 Sep 2018 | **Accepted:** 12 Jul 2019
Section Editor: William Wolf

Various studies have been reported on aerodynamic characteristics of aerofoil, especially from the experimental standpoint. On the contrary, comprehensive studies of wingtip model characteristics are less frequent in literature for aircraft, although their fundamental importance is acknowledged. In 1993, Tucker (1993) extensively investigated the split wingtips of soaring birds and demonstrated that the tip slots of soaring birds reduce the induced drag with increasing span factor of the wings. He observed significant improvements of slotted wingtips compared with conventional wing with a Clark Y airfoil, and investigated that as the same increase in angle of attack, the Clark Y tip increased the base wing drag by 25% while the feathered tip actually reduced the drag by 6%. Smith *et al.* (2001) examined the potential of multi-winglets for the reduction of induced drag without increasing the span of aircraft wings. The results show that certain multi-winglet configurations reduced the wing induced drag and improved lift/drag (L/D) by 15–30% compared with the baseline 0012 wing.

Miklosovic and Bookey (2005) experimentally assessed the effectiveness and efficiency of three winglets mounted chord wise to the tip of a rectangular wing (NACA 0018 section). They proved that the arrangements involving high dihedral angles had lower performance increments, due to lower lift and higher interference drag. More specifically, the results showed that the winglets could be placed in various optimum orientations to increase the lift coefficient as much as 65% at the same angle of attack, decrease the drag coefficient as much as 63% at the same lift coefficient, or improve the maximum L/D by up to 71%.

Winglets are known to improve the efficiency of large aircraft at high subsonic speeds, but winglet designs for smaller aircraft such as unmanned aerial vehicles (UAVs) are largely unproven. Ning and Kroo (2008) did a conceptual design optimization in tip extensions, winglets, and C-wings. C-wings are investigated for their potential to enhance performance beyond that offered by wings with winglets. The method is applied to wings with active load alleviation. Active load alleviation allows reductions in drag on the order of 15%.

Weierman and Jacob (2010) investigated methods for designing and optimizing winglet geometry for UAVs that operated at Reynolds numbers of about 10^6. Two types of winglet configurations have been analyzed which the configuration type 2 has improved lift over drag ratio up to 28.1%. Hossain *et al.* (2011a) studied the aerodynamic characteristics benefit of using aircraft model with and without winglet. Tests were conducted on the aircraft model with and without winglet using three configurations at Reynolds numbers 1.7×10^5, 2.1×10^5, and 2.5×10^5 for different angle of attacks. It is mentioned that elliptical winglet with 60° inclination has the best performance, giving about 6% increase in lift curve slope as compared to without winglet.

Khosravi and Zingg (2014) focused on the design optimization of a winglet to find out whether upward or downward winglet design will give best outcome. Guezguez *et al.* (2016) designed and manufactured a morphing wingtip in order to optimize the aerodynamic configurations. They validated their data with wind tunnel tests and the results show that their integrated hardware design of systems has produced a faster method to link several wing peripherals with different signals to the controller unit. Kammegne *et al.* (2017) proposed new control methodology for morphing wing to improve the aircraft aerodynamic performance. Their technique performed very well during wind tunnel testing and the static errors achieved were less than 0.1 mm with overshoots were less than 5% of static values. Pratilastiarso *et al.* (2018) carried out experimental study on the wind turbine with split winglets added on their blades. The experimental results indicated that the backflow on the tip of blades was minimized and the best performance was achieved among all the turbine variations when the split winglets were added on the turbines. Jones *et al.* (2018) used the periodic surface morphing to control the suction side of an airfoil which intermittently morphed at several frequencies. They found that the large coherent structures created the extra momentum caused by the spectra actuation frequency and successfully decrease the separation area.

The numerical study on winglet performance rarely found in literature with previous studies focused only on the experimental works. Ashrafi and Sedaghat (2014) conducted numerical simulation on the NACA 65-218 airfoil with and without winglet. They studied the effect of utilization of a winglet on a NACA 65-218 airfoil to improve the aerodynamic performance of a wing. Their results show that better lift coefficient and higher lift/drag ratio were achieved when the simple and semicircular winglet (45° cant angle) was added to the wing. The 3D aerodynamic analysis for various configurations for airplane wingtip with split winglets have been investigated by Reddy *et al.* (2016). The split winglet configuration with the addition of scimitar tip spikes further increases the wingtip vortex core radius and better redirected the flow to reduce the induced drag. This

opens a possibility of optimizing split winglets with multiple elements mimicking a soaring bird's wingtip spread feathers like RGV wingtip. Gabor *et al.* (2016) investigated a morphing wing equipped with a flexible upper surface and controllable actuated aileron. The model which was fitted with a composite material upper skin whose shape can be morphed as a function of the flight condition, by four electrical actuators placed inside the wing structure are used. With the aim of controlling the extent of the laminar flow region, the optimizations were performed and the resulting shapes were scanned using high-precision photogrammetry. Another study on controllable aerodynamic performance on the morphing wing is conducted by Wu *et al.* (2017) who have been using a combination of linear ultrasonic motors (LUSMs) with an innovative morphing structure. They found that higher L/D ratio is achieved for all morphing states when the aerofoil camber is increased. Gabor (2017) performed a numerical study for a nonlinear constrained aerodynamic optimization problem. They used a numerical nonlinear lifting line method in order to optimize the winglet toe angle for morphing winglets. Their results yield a better computational calculation time in terms of the total number of linear system solutions. Eguea *et al.* (2018) reported the aerodynamic performance optimization of the airfoil with winglets by using BLWF code. They found that camber morphing winglet type have increased the aerodynamic performance and reduced the total drag up to 0.58% when compared to the fixed geometry winglet. Abdessemed *et al.* (2018) conducted a numerical study of the NACA 0012 airfoil which focused on high frequency and low amplitude configurations for the harmonically morphing trailing edge flap (TEF). Their results show that aerodynamic efficiency was increased up to 3% when the morphing frequency was fixed at its shedding value. Munshi et al. (2018) investigated the effect of winglet cant angle at different angles of attack from 3° to 6° on the ONERA M6 wing by using the ANSYS Fluent. Their numerical outcomes exhibited the C_L/C_D ratio improvement up to 25% in transonic regime when an aircraft wing with winglets compared to the wing without winglets. However, the performance dropped when the angle of attack was increased to 6°.

The Rüppell's griffon vulture (RGV) is the highest-flying bird in the world, with confirmed evidence of flights at an altitude of 11,300 m (37,000 ft) above sea level (Laybourne 1974) as shown in Fig. 1, has been taken as the main consideration for the winglet design in this research. Modifying wingtip is much easier and cheaper in aircraft industries compared to changing the whole wing. That is the main reason of why the focus is only on the RGV winglet and not its wing. This research has a fixed chord and thickness of NACA \$65(3)-218 airfoil and a constant Reynold's number.

Figure 1. The Rüppell's griffon vulture wingtip feathers.

OBJECTIVES

The hypothesis of the authors of this work is that RGV winglet will reduce induced drag, which is one of the major contributions of the total drag and reduce wake vortex formation. To the best knowledge of the authors, the study of RGV winglet has never been done before. This pioneering study is to design the best nature flyer (RGV bird) with the hope that it will provide an alternative for the future of the aircraft industry. This research aims to design a model wing with RGV winglet and study its performance with the help of ANSYS software. Furthermore, it is extended to study effect of cant angle and different angles of attack (AOA) to the winglet. Both numerical simulation and an independent experimental work

done by Hossain et al. (2011b) will be compared in order to enhance the validity of the current study. Simulation results will be analyzed based on aerodynamic performance to find out the best RGV winglet with best AOA for contour plot analysis comparison with wing.

METHODOLOGY

GOVERNING EQUATIONS

In the simulation model, the incompressible Navier–Stokes equations are considered for describing the air flow due to the low speed flow. The governing equations describing the fluid flow are conservation of mass and conservation of momentum. The conservation of mass equation is given by:

$$\frac{\partial u_i}{\partial x_i} = 0 \tag{1}$$

where: u_i is the fluid velocities with the density of air deemed constant. The conservation of momentum is written for an inertial reference frame and is described by:

$$\frac{\partial}{\partial t}(u_i) + \frac{\partial}{\partial x_j}(u_i u_j) = -\frac{1}{\rho}\frac{\partial P}{\partial x_i} + \frac{\partial \pi_{ij}}{\partial x_j} + g_i + F_i \tag{2}$$

where: P is the static pressure, τ_{ij} is the viscous stress tensor and g_i and F_i are the gravitational acceleration and external body force in the i-direction, respectively.

The shear-stress transport (SST) k-ω solver was utilized for all of the turbulence model investigations described in this work. The model is chosen due to it is typically designed for boundary layers resolution problem, more accurate and robust compared to other turbulence models as demonstrated by Menter (1994).

The SST k-ω model solves the two transport equations for k and ω which are the turbulence kinetic energy and the dissipation rate respectively. They are obtained from transport equation and given as follows:

$$\frac{\partial}{\partial t}(k) + \frac{\partial}{\partial x_i}(k u_i) = \frac{\partial}{\partial x_j}\left(\Gamma_k \frac{\partial \mathrm{k}}{\partial x_j}\right) + G_k - Y_k + S_k \tag{3}$$

$$\frac{\partial}{\partial t}(\omega) + \frac{\partial}{\partial x_i}(\omega u_i) = \frac{\partial}{\partial x_j}\left(\Gamma_\omega \frac{\partial \omega}{\partial x_j}\right) + G_\omega - Y_\omega + D_\omega + S_\omega \tag{4}$$

In this study, the enhanced the wall treatment model approach is used to capture the behavior of flow near the wall which has a no-slip condition. This effect has a significant impact on the fidelity of numerical solutions.

COMPUTATIONAL FLUID DYNAMICS (CFD) MODELLING

The numerical study was performed in a three-step process which includes pre-processing, processing, and post-processing. The pre-processing step included geometry and meshing setup. The computational model is developed based on the NACA 65(3)-218 aerofoil (Fig. 2) by using commercial ANSYS workbench. In the first part of the study, the rectangular wing with different configurations are evaluated. Figure 3 depicted the type of wing configuration used in this study.

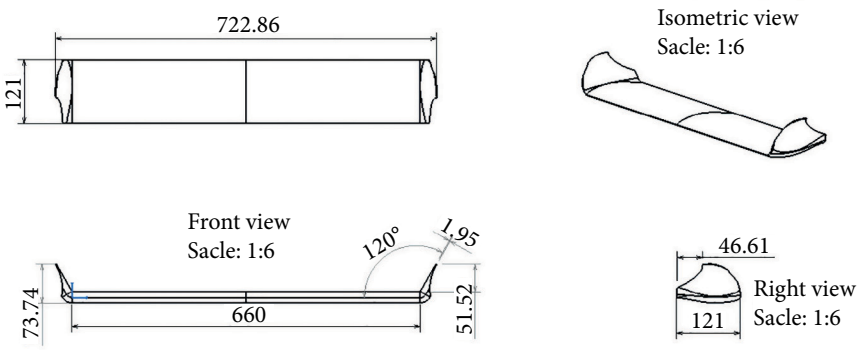

Figure 2. NACA 65(3)-218 aerofoil model.

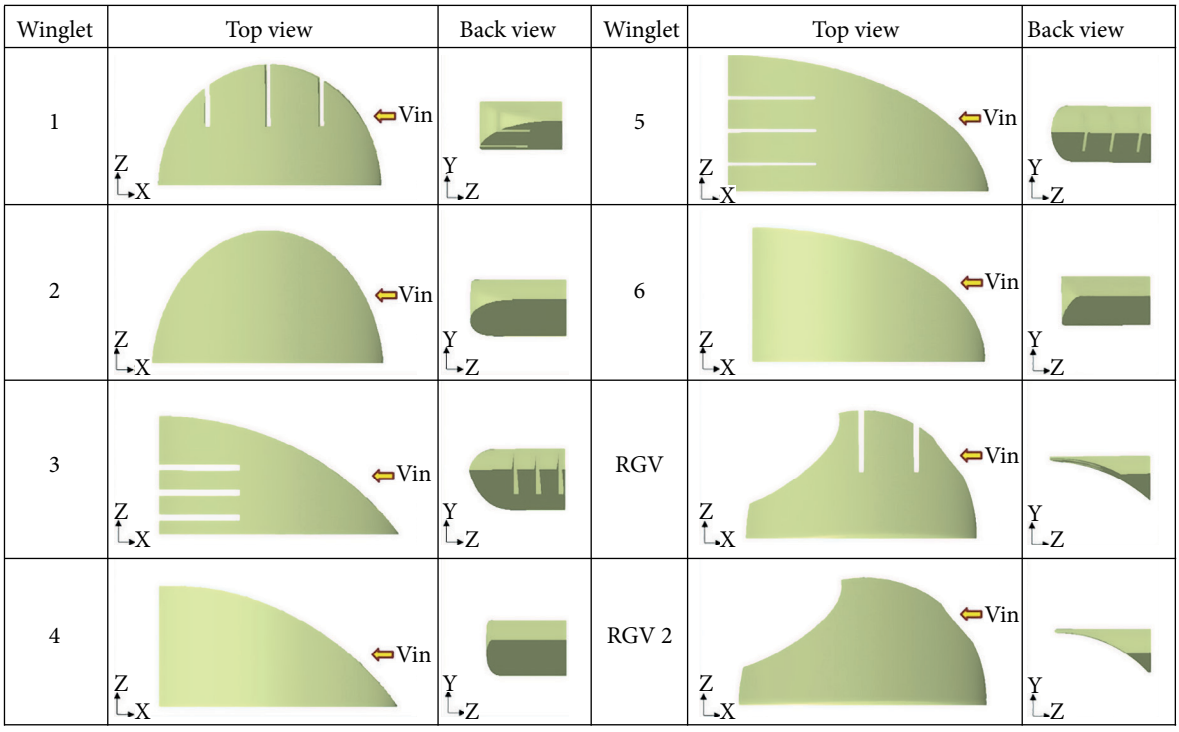

Figure 3. Type of winglet configuration.

At first, different cant angles were studied to find the best cant angle which gives higher aerodynamic performance for a winglet. The cant angle range in between –90° to 90° was performed with reference to the diagram depicted in Fig. 4. Only winglet (1) design was chosen to perform the cant angle test due to a much easier comparison with Hossain *et al.* (2011b) that used the same type of wing. The setup is covering for two steps of angles on this rectangular wing, which are at 0° and 60°. Figure 4(a), (b) and (c) shows the orientations of winglet blended as wingtip on an aircraft wing model. Each of these orientations config.d different cant angles from 90°, 60° of the upper side (positive) and 90° down side (negative) on the wing structures. The winglet type 1 then will be selected for further analysis by varying the cant angle values ranged from 90° to –90°.

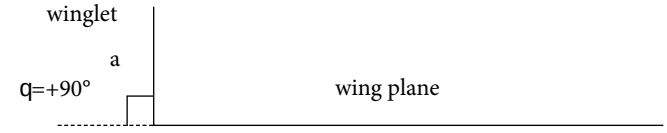

(a) Cant angle configuration at +90°

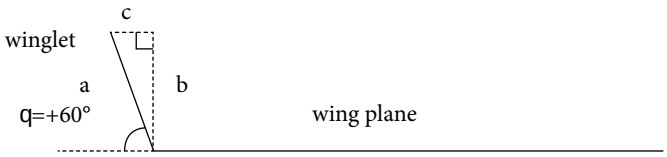

(b) Cant angle configuration at +60°

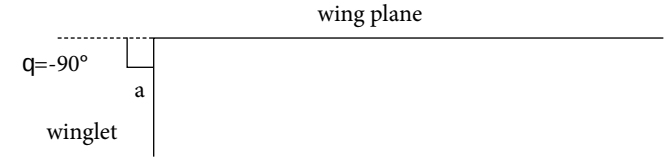

(c) Cant angle configuration at -90°

Figure 4. Cant angle configurations.

Then, the different configurations of the winglet were studied based on the angle of attack (AOA) from range 0° to 14° in order to study the discrepancies of performances of different winglets. The winglet model is meshed using unstructured triangular meshing method in all simulation work presented here. This method was selected because of its capability to capture near-wing and winglet complexity with relative ease and created a very fine grid near the boundary layer with y+ ~1. Note that Reynolds number 2.5×10^5 is used for both the simulation and experimental set up. Figure 5 shows the overall mesh produced from the model with the boundary conditions. Face meshing size is set to 2 mm where else the growing prism inflation layer option has been implemented on the wing boundaries with the first adjacent cell above wall set at 0.0001 m with 20 layers in a growth rate set to 1.108 as shown in Fig. 6. The mesh element size close to the wing and winglet was smaller and moving towards the domain boundary walls, the element size incrementally increased as shown in Fig. 7.

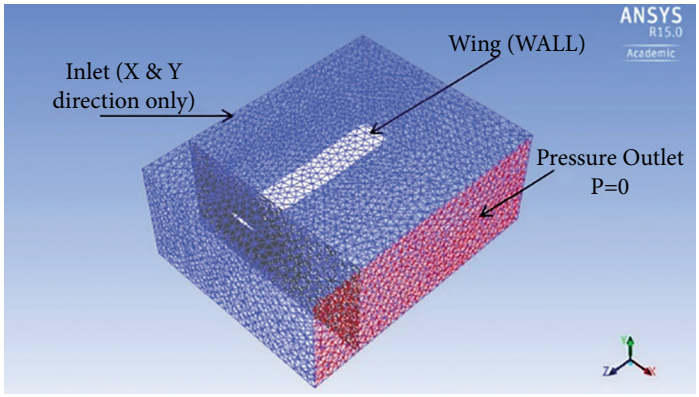

Figure 5. Computational mesh with boundary conditions setup.

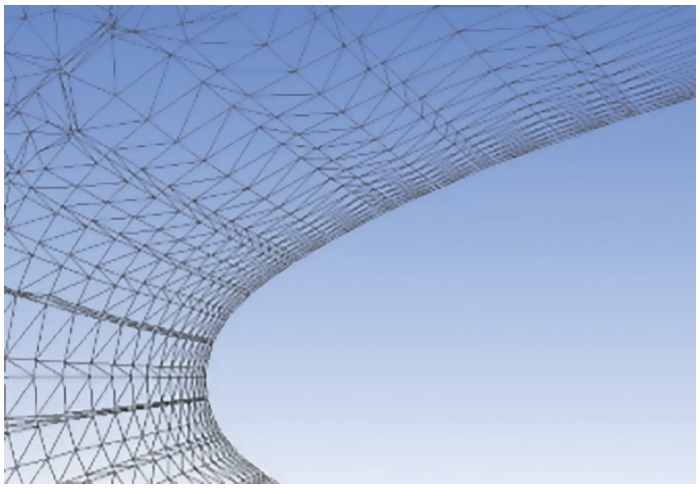

Figure 6. Boundary inflation with refined mesh near the wing.

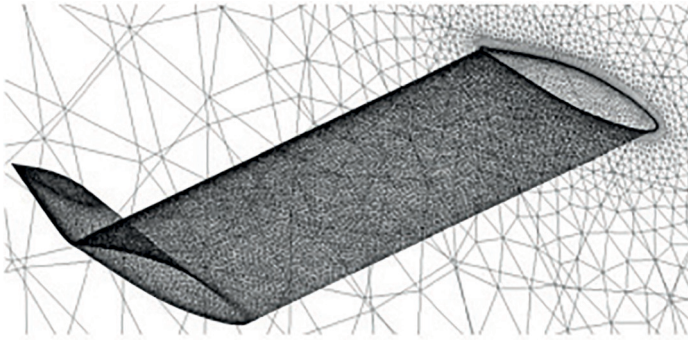

Figure 7. Finer mesh around wing.

The wing model with domain consists of about 1,500,000 elements, which was very effective in terms of computational time as well as the results quality. Velocity inlet is selected as inlet boundary condition and pressure outlet for the outlet boundary. The boundary condition for wing and domain are set as no-slip boundary conditions. The shear-stress transport k-ω model is used as the simulation model in this study. The momentum and pressure equations are solved by the implicit solver. The SIMPLE scheme and second-order upwind discretization were selected for pressure-velocity coupling. The convergence ratio and residual error are set to be in the order of 10^{-3} to 10^{-4}. The pressure (P) is defined as the relative pressure to the standard atmospheric pressure (1 atm). Thus, the initial boundary conditions are listed as follows:

- At inlet gate: $P=P_{inlet(x,y,z,t)}$
- On wall boundary: $u = v = w = 0; \frac{\partial p}{\partial n} = 0$
- At outlet gate: P=0 (relative to atmospheric pressure)

GRID INDEPENDENCE TESTS

A grid independence test was done to reduce the influence of the number of grid size on the computational results. This test is usually executed for the simulation analysis in order to find the sufficient number of mesh elements. Table 1 and Fig. 8 show the

results of the grid independence test for different type of grid resolution of mesh from low to extra fine. From the data analysis results, the optimum mesh is the mesh resolution that has the lowest discretization error and is also the most cost effective in terms of computational time. As Fig. 7 shows, the optimum mesh grid used in this research is the fine mesh with 1,510,734 number of grid cells. This mesh grid is chosen due to the optimal simulation accuracy and low execution time.

Table 1. Summary of grid independence test.

Mesh model	Grid resolution	Number of cells	Lift coefficient C_L	Discretization error (%)
1	Low	250,325	0.116	44.26
2	Medium	750,734	0.164	26.79
4	Fine	1,510,838	0.220	2.22
5	Extra fine	2,002,011	0.224	1.78
6	Extra fine	2,556,311	0.225	–

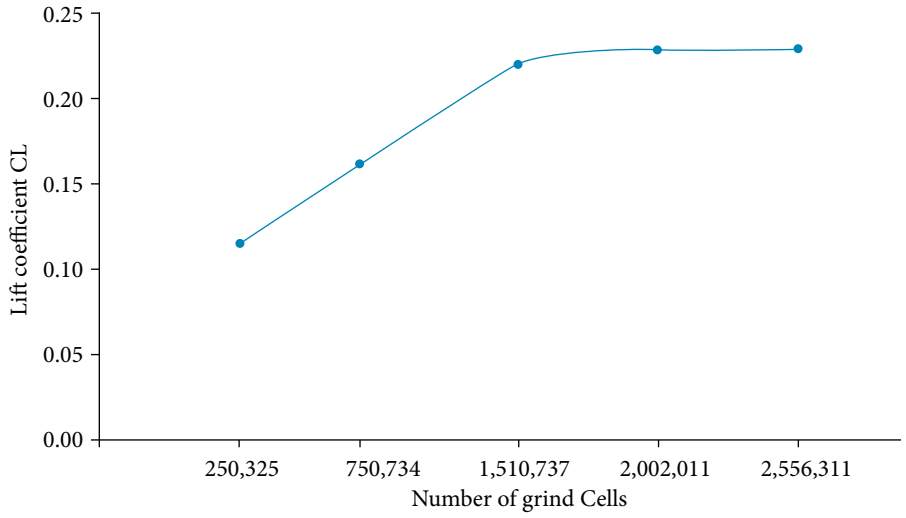

Figure 8. Graph lift coefficient C_L at AOA 0° versus number of grid cells.

RESULTS AND DISCUSSION

MODEL VALIDATION

For verification purposes, the experimental results of Hossain *et al.* (2011b), who used winglet design type 1, which has the same span and chord length as in the present numerical study, were compared with the simulation results. Based on the technique presented above, a simulation system has been established with ANSYS fluent. The RGV winglet lift coefficient (C_L) and (C_D) by simulation is compared with the experimental results. In this model validation, the winglet design has a span of 0.66 m and a chord of 0.121. The process parameter settings in FLUENT are according to the actual experiment settings as stated by Hossain *et al.* (2011b). The lift coefficient and lift coefficient/drag coefficient experimental results and FLUENT simulation are plotted in Fig.s 9 and 10, respectively.

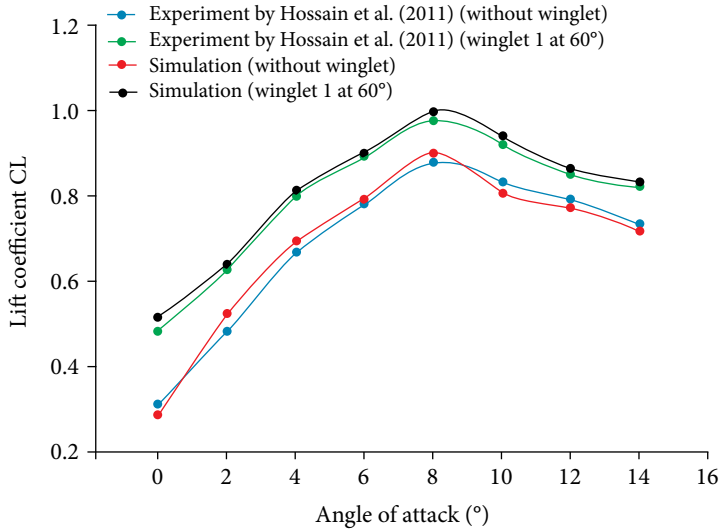

Figure 9. Graph lift coefficient versus AOA for without winglet and winglet (1) by experiment and simulations for Reynolds number 2.5 × 10^5.

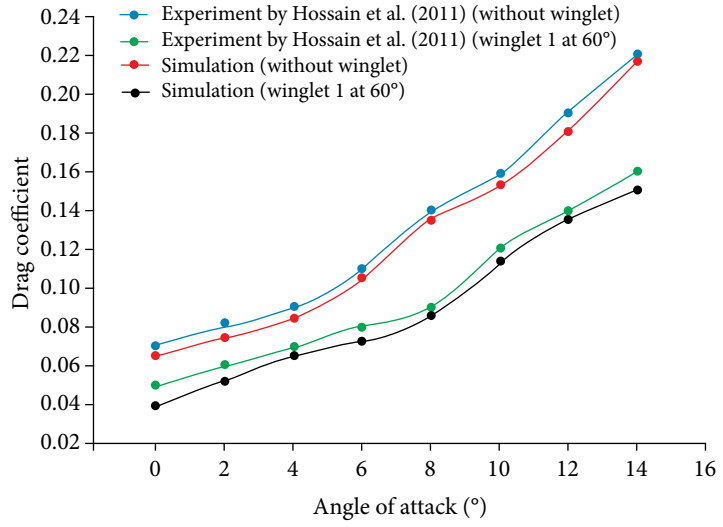

Figure 10. Graph drag coefficient versus AOA for without winglet and winglet (1) by experiment and simulations for Reynolds number 2.5 × 10^5.

As can be seen in Fig. 9, a close agreement between an independent experimental results and simulation is exhibited. There is an average discrepancy of 8.64% between the experimental and simulation results for the case without winglet whereas 8.91% was calculated for the winglet (1) case. Furthermore, the drag coefficient experimental and simulation results exhibited nearly identical trend (Fig. 10). Therefore, the feasibility of using FLUENT in simulating winglet performances (lift coefficient and drag coefficient) has been proven.

CANT ANGLE WINGLET ANALYSIS

Figure 11 shows winglet (1) at positive cant angle 60° result, which is 0.6841, where else winglet at negative cant angle −90° result is 0.600. All the C_L results at negative cant angles from −15° to −90° are lower than 0.67 in comparison with C_L at positive angles which are higher than 0.67. This is the main reason why most of the winglet design configuration is upwards (positive cant angle) rather than downwards (negative cant angle). The velocity contour profiles for various cant angles are depicted in Fig. 12.

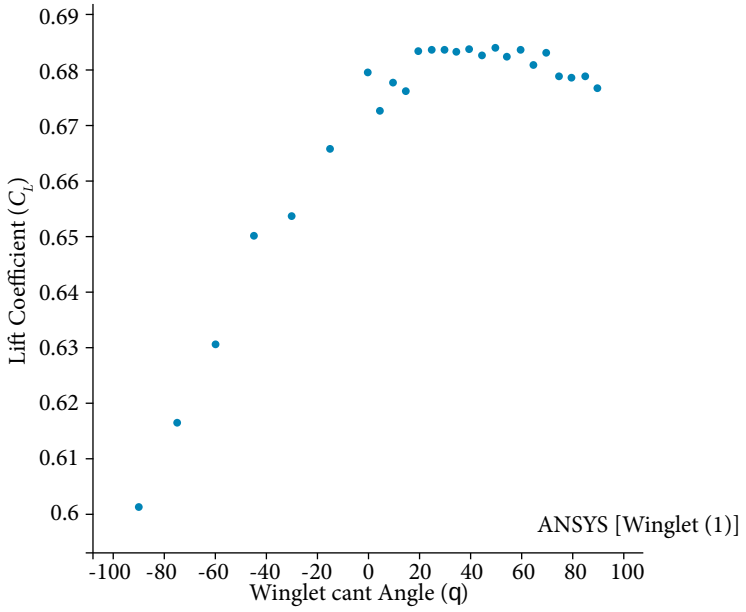

Figure 11. Graph lift coefficient versus cant angle for AOA 4° with Reynolds number 1.7 × 10^5.

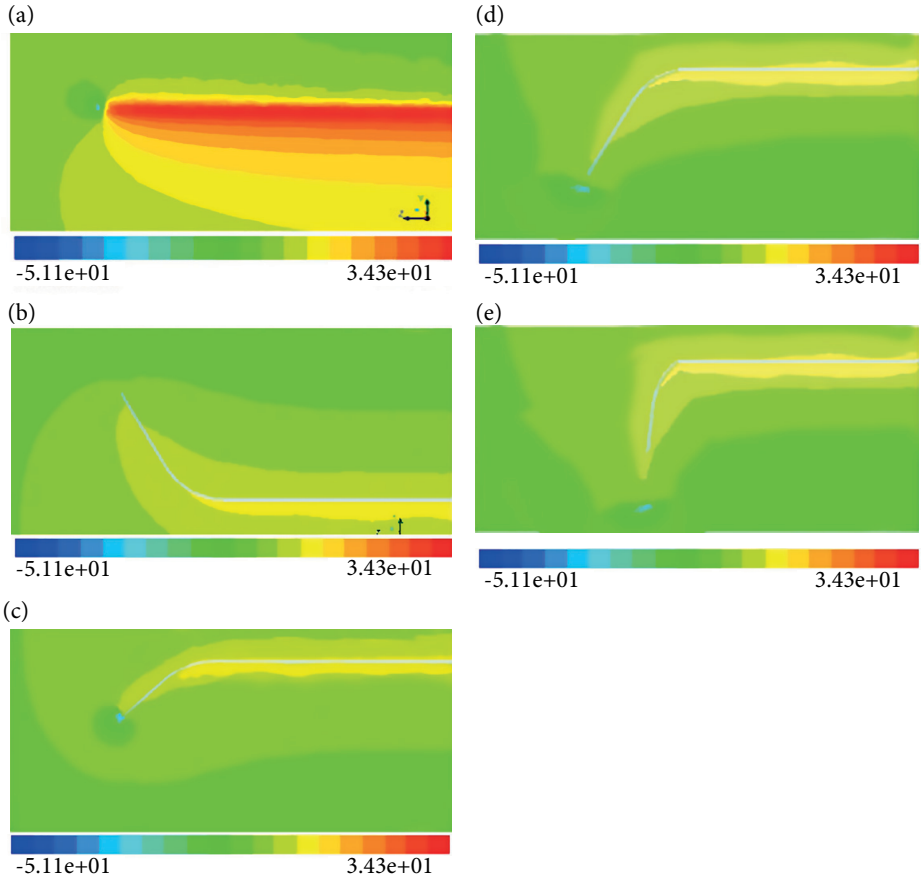

Figure 12. Pressure coefficient and velocity magnitude for winglet (1) at AOA 4° with cant angle; (a) 0°; (b) 60°; (c) -30°; (d) -60°; (e) -90°.

Figure 13 shows the lift coefficient and Fig. 14 shows the lift coefficient/drag coefficient versus AOA for different winglet configurations by experiment and simulations for Reynolds number 1.7×10^5. There is a clear trend of increasing C_L/C_D for all winglet configurations until AOA is reached 4°. However, the C_L/C_D started to decrease after AOA achieved 8° due to the flow separation of air phenomenon. Maximum lift/drag ratio output results are winglet (4) and experiment by Hossain *et al.* (2011b) which are 11.111 and 11.27 respectively at 4° of AOA. Winglet (RGV (2)) shows second highest result which is 10.99 at 4° of AOA. Further analysis revealed that the RGV (2) winglet decreases C_D output to 15 to 30% and increases lift/drag ratio up to 25 to 75% compared to other type of winglets configuration.

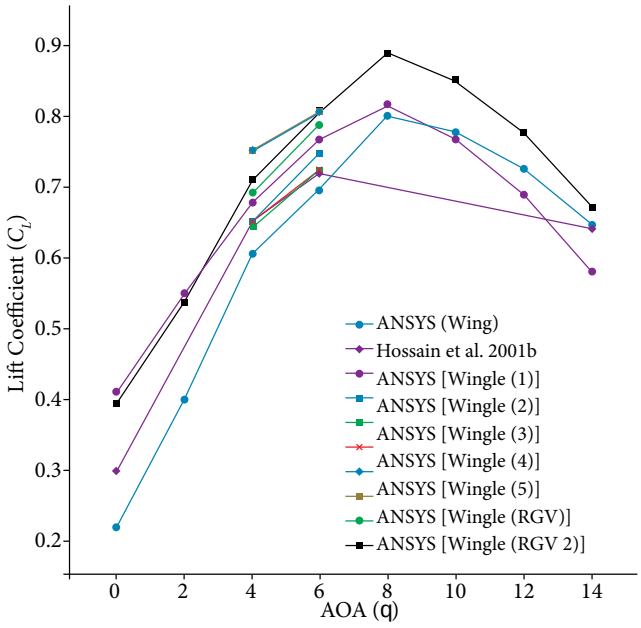

Figure 13. Graph lift coefficient versus AOA for different winglet configurations by Hossain *et al.* (2001b) and simulations for Reynolds number 1.7×10^5.

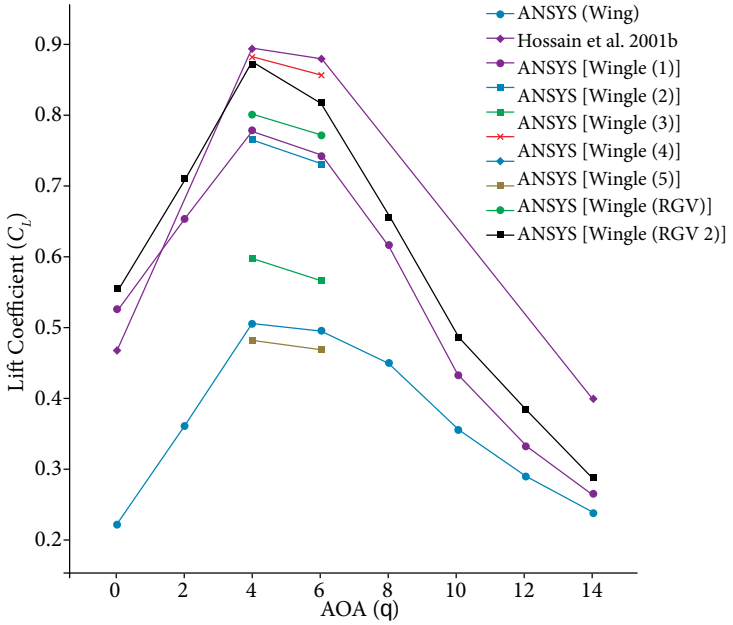

Figure 14. Graph lift coefficient/drag coefficient versus AOA for different winglet configurations by Hossain *et al.* (2011b) and simulations for Reynolds number 1.7×10^5.

Velocity and pressure analysis

When a free stream velocity flows over an air foil, there will be high velocity at top surface meanwhile low velocity at the bottom. According to Bernoulli's principle, high velocity will cause low pressure and low velocity will cause high pressure. This high pressure on the bottom surface of the wing, causes air to accelerate towards the low-pressure region on the top surface of the wing near the wingtip which causes a downwash effect or wingtip vortex. On the other hand, the adverse pressure gradient slows down the velocities inside the boundary layer. In other words, this pressure variation will cause bending moment at the edge of the wingtip where the vortex formation is formed. This wingtip vortex keeps growing as much as the air is accelerated from the bottom to the upper wing surface. Even after leaving the wing trailing edge, the wingtip vortex continues to grow as spanwise wing vorticity is entrained (Anderson 2004). The predicted pressure and velocity magnitude profiles are studied for the wake vortex formation in the cross-flow from planes 5 to plane 8, which are shown in Fig. 15.

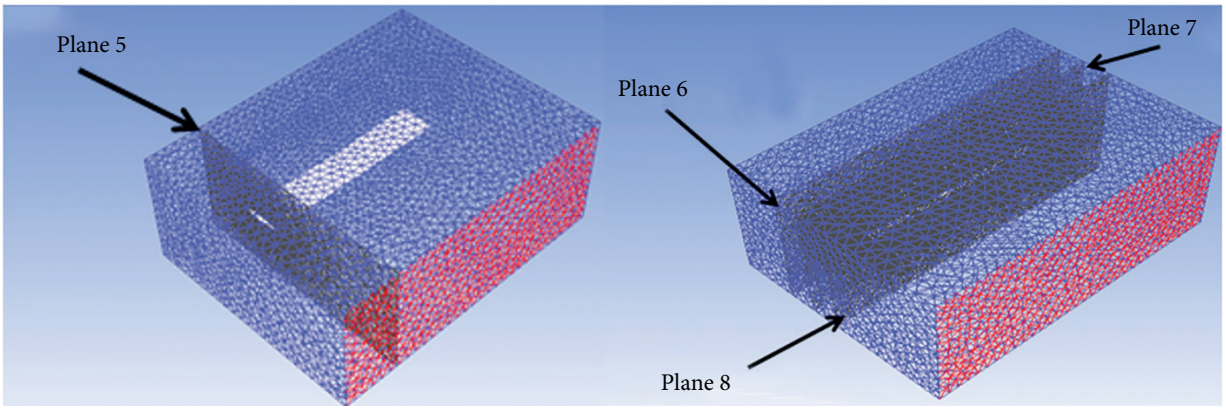

Figure 15. Plane 5 to 8 at different locations of winglet.

EFFECT OF WINGLET TO THE VELOCITY

Figure 16 presents the velocity magnitude distribution plot at plane 5 for the AOA 4° and 8°. A comparison with both results reveals the vortex formation on the wing is high compared to RGV (2) for both AOA 4° and 8°. The addition of the winglet to the wing has reduced the vortex formation. This is because the RGV (2) winglet decreased the vortices of the wing which is created by the pressure difference between upper and lower surface of wing. The lower pressure on the upper surface creates a natural airflow that flow through the winglet and curls downward around it.

Figure 17 shows the velocity magnitude distribution plot at plane 6 for the AOA 4°. There is a vortex formation seen at the end of aerofoil edge for wing type, meanwhile the RGV (2) and winglet (6) exhibited a smooth flow at the aerofoil. The reason of this condition is due to a velocity break at the edge. The velocity at the bottom surface is higher than that at the top surface. Therefore, such difference in velocity creates the vortices at the edge of the aerofoil.

Figure 18 compares the velocity magnitude distribution plot at plane 7 for all winglet configurations at AOA 4°. Since this plane is at the center (in chord or x-direction) of an airfoil, the vortex formation can be seen much clearer. In this research, plane 7 can be considered as one of the best cross-section planes to discuss velocity distribution analysis in details when compared to other planes. It can be seen from the data in Fig. 18 that wake vortex formation generated for all type of winglet except RGV and RGV (2). This is because of the smooth velocity or continues flow is produced with the winglet design RGV. Other types of winglet design illustrated the velocity discontinuity that caused the circulation around the aerofoil which has created vorticity around the wing. Furthermore, the RGV and RGV (2) winglet exhibited low vorticity at the tip region. The addition of winglet RGV or RGV (2) substantially reduces the strength of the vortices at the wingtips. As discussed in Fig. 11, where winglet RGV (2) gives the highest lift/drag ratio, shows the contour plot with less vorticity occurrence towards to the wingtip, the lowest lift/drag ratio, wing with winglet 5 and 6 shows the highest formation of vorticity at the edge wing.

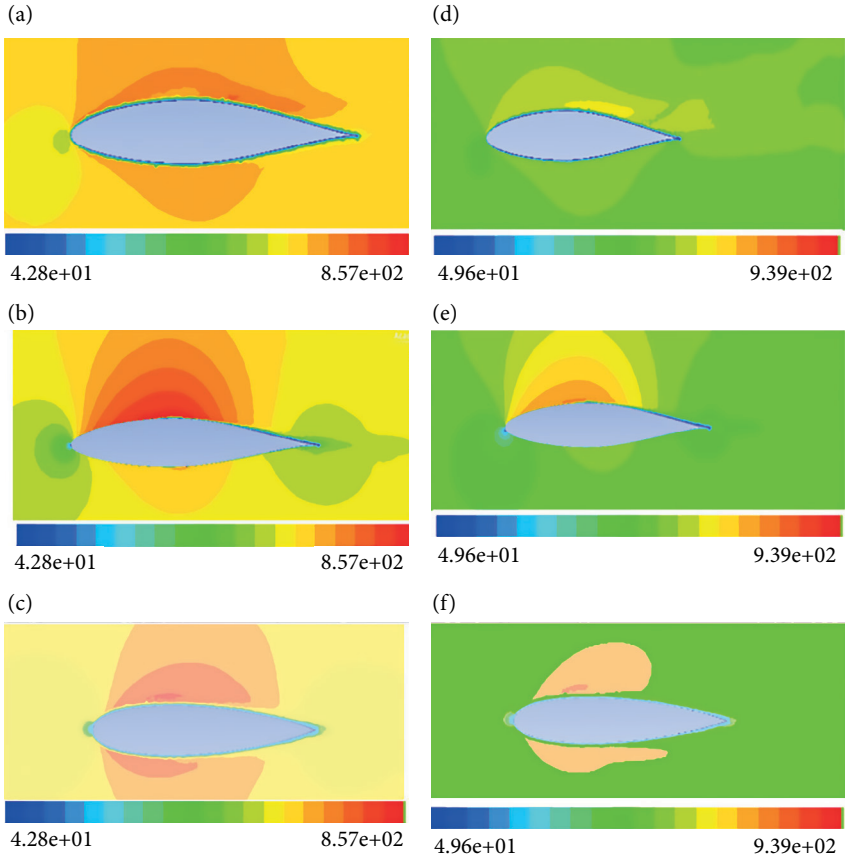

Figure 16. Velocity magnitude for wing, RGV (2) and winglet (6) (AOA 4° and 8°) at plane 5. AOA: (a) Wing - 4°; (b) RVG 2 - 4°; (c) Winglet (6) - 4°; (d) Wing - 8°; (e) RVG 2 - 8°; (f) Winglet (6) - 8°.

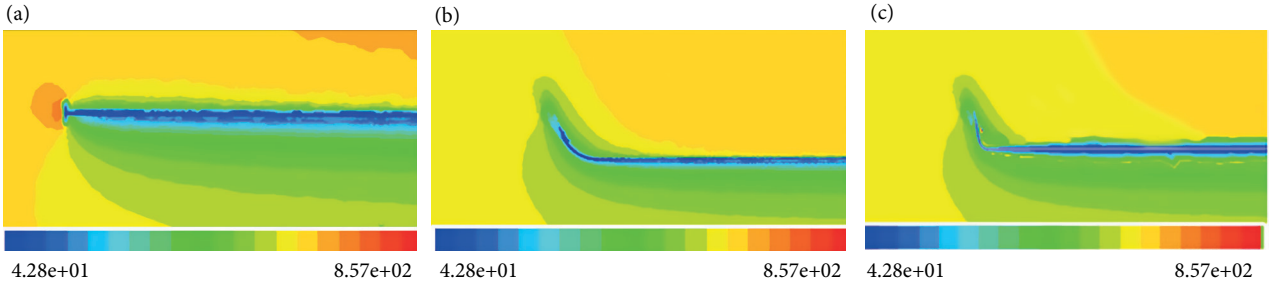

Figure 17. Velocity magnitude for wing, RGV (2) and winglet (6) at AOA 4° at plane 6. AOA: (a) Wing; (b) RVG 2; (c) Winglet (6);

The results obtained from the velocity magnitude distribution plot at plane 8 for the AOA 4° and 8° are compared in Fig. 19. It is apparent from this fig. that there is still high vortex formation at aerofoil for wing for both AOA 4° and 8°. Further analysis showed that RGV (2) formed smooth flow without any vortex formation compared to winglet (6) and wing. Hence, the addition of winglet RGV (2) has proved to reduce the vortex formation on the aerofoil.

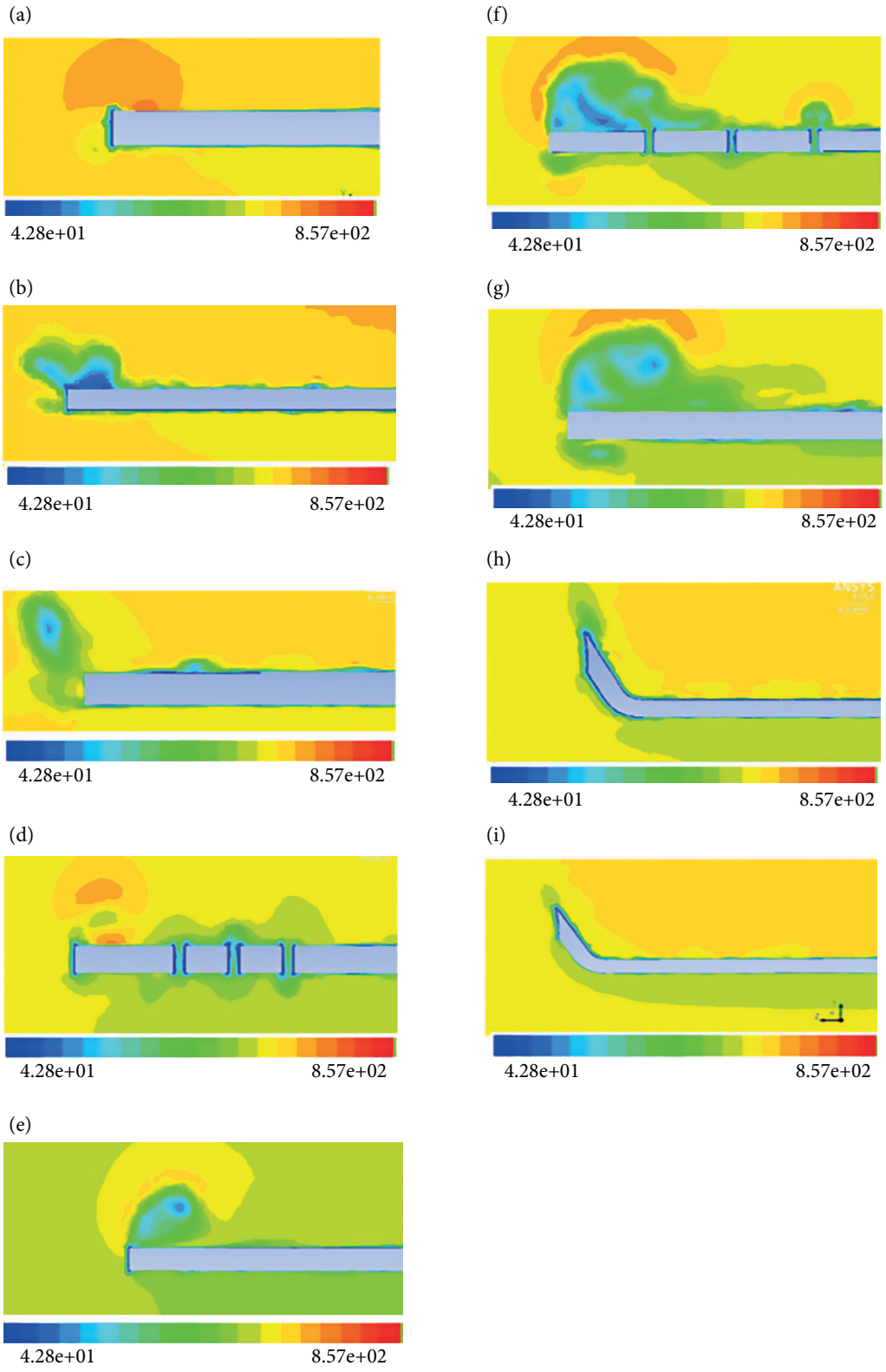

Figure 18. Velocity magnitude for all winglet configurations at AOA 4° at plane 7. Winglet: (a) Wing; (b) 1; (c) 2; (d) 3; (e) 4; (f) 5; (g) 6; (h) RVG; (i) RVG 2.

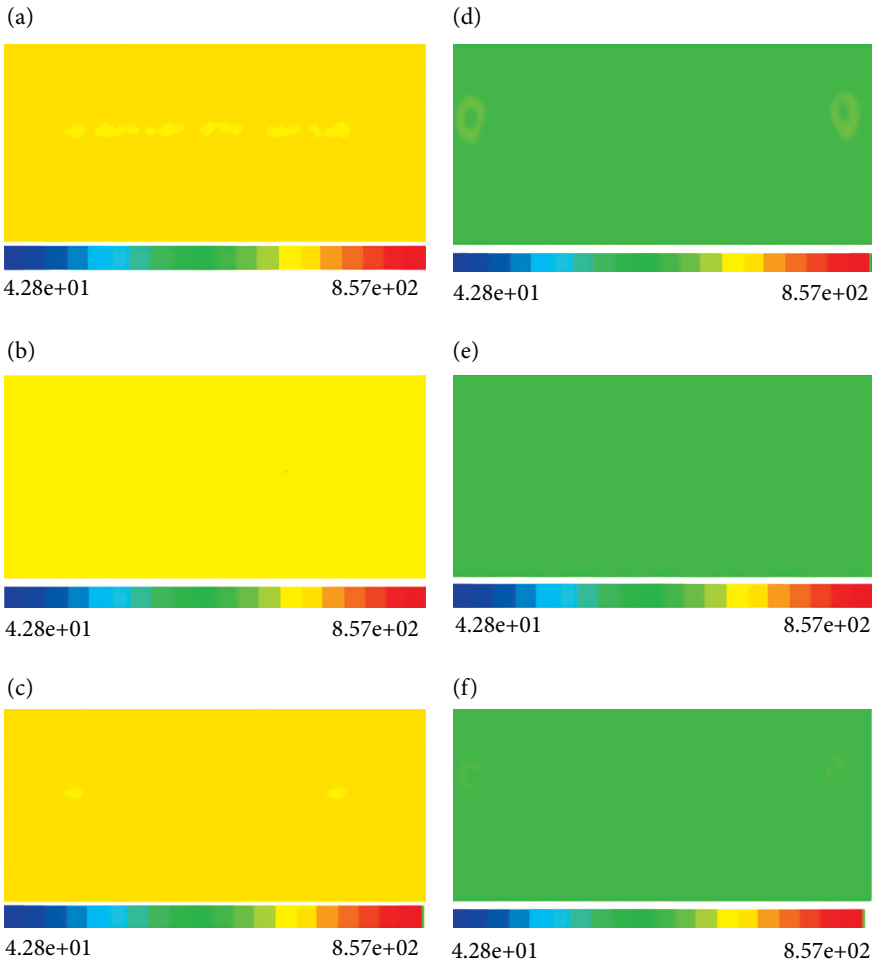

Figure 19. Velocity magnitude for wing, RGV (2) and winglet (6) at AOA 4° and 8° at plane 8.
AOA: (a) Wing - 4°; (b) RVG 2 - 4°; (c) Winglet (6) - 4°; (d) Wing - 8°; (e) RVG 2 - 8°; (f) Winglet (6) - 8°.

EFFECT OF WINGLET TO THE PRESSURE

Figure 20 shows the pressure coefficient distribution at plane 5 for wing, RGV (2) and winglet (6) configuration (AOA 4° and 8°). When there is no winglet at the edge of the wingtip, there is a pressure lost corresponding at the beginning (creation) of the vortex. The pressure distribution becomes steady after the RGV (2) winglet is added to the wing compared to wing and winglet (6).

Figure 21 provides the pressure coefficient distribution at plane 6 for wing, RGV (2) and winglet (6) configuration (AOA 4°). There is a vortex formation at the edge of wing only whereas RGV (2) and winglet (6) did not have vortex formation. The addition of winglet (RGV2) reduced the vortex formation which in turn reduces drag and increases lift for the wing. The decreasing of pressure coefficient trend indicates that airfoil starts to experience stall as the lower surface gradually having similar pressures to the upper surface. Generally, there is a high pressure below and low pressure on top of a wing with winglets. Without winglet, the pressure on top is not much difference with pressure below hence loss of lift.

Figure 22 shows the pressure coefficient distribution at plane 8 for wing, RGV (2) and winglet (6) configuration (AOA 8°). The large formation of vortex can be seen on wing whereas there is less vortex generated when using winglet (6), followed by RGV (2) winglet. In this study, the wing and winglet (6) type was found to cause the vortex formation that may reduce the aerofoil performance. Figure 22 shows the induced vortex strength is reduced with RGV winglet.

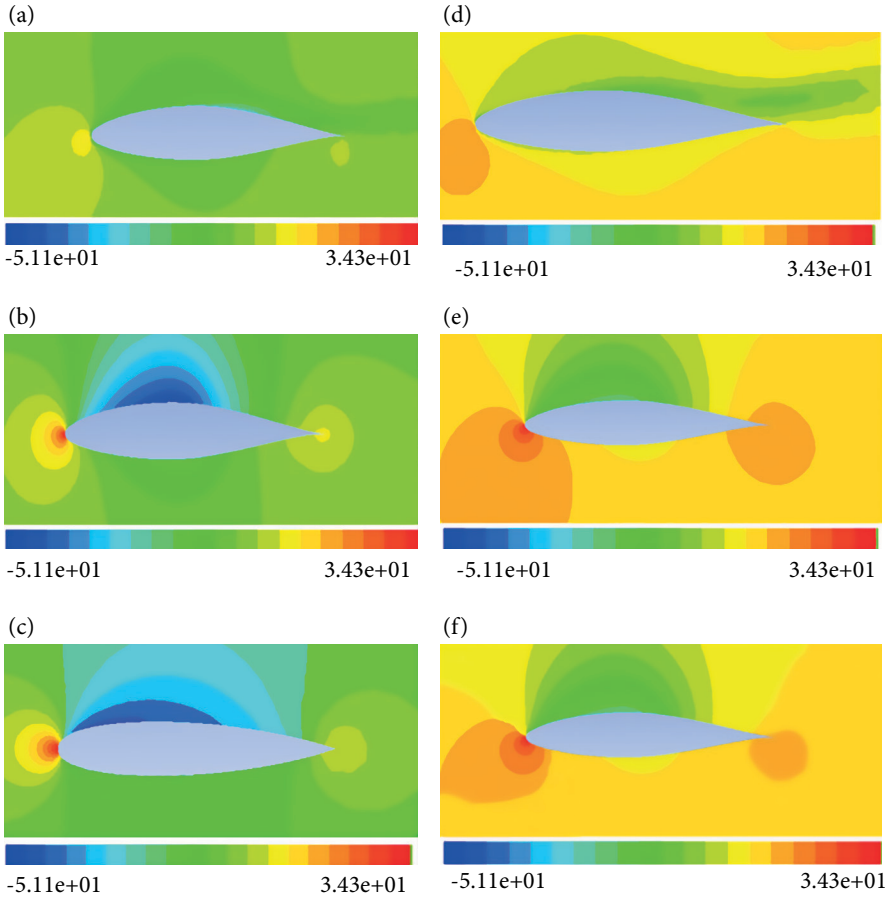

Figure 20. Pressure coefficient for wing, RGV (2) and winglet (6) at AOA 4° and 8° at plane 5. AOA: (a) Wing - 4°; (b) RVG 2 - 4°; (c) Winglet (6) - 4°; (d) Wing - 8°; (e) RVG 2 - 8°; (f) Winglet (6) - 8°.

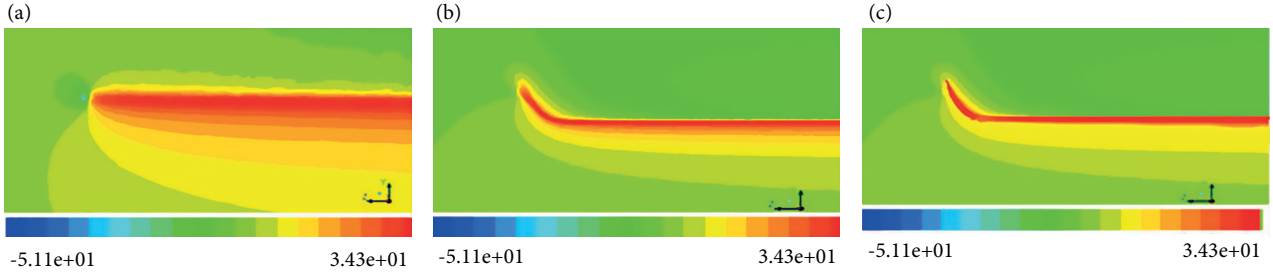

Figure 21. Pressure coefficient for wing, RGV (2) and winglet (6) at AOA 4° at plane 6. (a) Wing; (b) RVG 2; (c) Winglet (6).

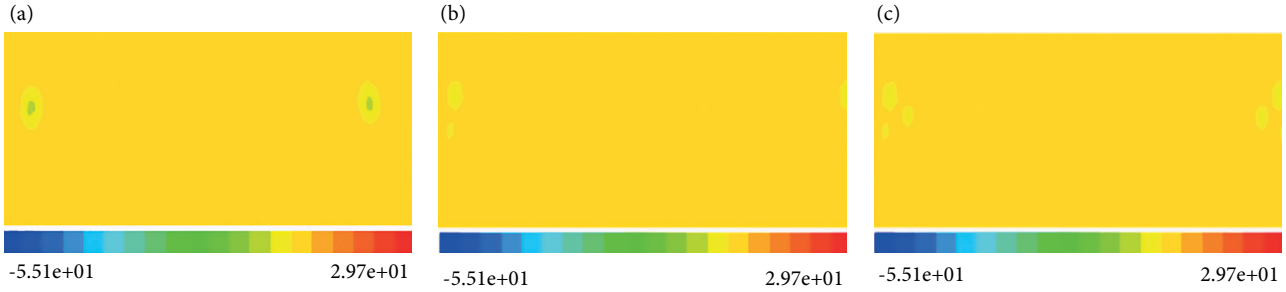

Figure 22. Pressure coefficient for wing, RGV (2) and winglet (6) at AOA 8° at plane 8. (a) Wing; (b) RVG 2; (c) Winglet (6).

CONCLUSIONS

The numerical study of winglet performance has been done by comparing eight types of winglet design. The simulation is validated against independent experimental results. This study has shown that positive cant angles have better performance due to their higher C_L results compared to negative cant angles. 60° cant angle is considered the best cant angle and it is used for all design configurations. For most of the conditions, the maximum C_L result is achieved with the RGV2 winglet, for instance $C_L = 0.89$ for AOA 8°. In addition, the RGV (2) winglet shows a very good performance in terms of C_L/C_D in comparison with other winglets. For example, at 4° AOA of $C_L/C_D = 10.99$, which is the second highest among all winglets. Overall, the results of this investigation show that the RGV (2) winglet increases C_L output up to 5 to 25%, decreases C_D output to 15 to 30% and increases lift/drag ratio up to 25 to 75% compared to other type of winglets configuration. Lastly, the current numerical simulation method offers superior visualization and understanding of the performance during winglet design, particularly using RGV-type winglets.

ACKNOWLEDGMENTS

Editors and authors are thankful to Fundação Conrado Wessel for providing the financial support for publishing this article, and also to all the reviewers for providing a very constructive feedback to this paper.

FUNDING

Universiti Sains Malaysia Research University. Grant 1001.PAERO.8014091
[http://dx.doi.org/10.13039/501100004595]

AUTHOR'S CONTRIBUTION

Conceptualization, Krishnan SG and Ismail F; Methodology, Krishnan SG and Ishak MH; Investigation, Krishnan SG, Ishak MH and Nasirudin MA; Writing – Original Draft, Krishnan SG and Ismail F; Writing – Review and Editing, Ishak MH, Nasirudin MA and Ismail F; Funding Acquisition, Ismail F; Resources, Ishak MH and Ismail F; Supervision, Ismail F.

REFERENCES

Abdessemed C, Yao Y, Bouferrouk A, Narayan P (2018) Aerodynamic analysis of a harmonically morphing flap using a hybrid turbulence model and dynamic meshing. In: 2018 Applied Aerodynamics Conference. Atlanta: AIAA Aviation Forum. https://doi.org/10.2514/6.2018-3813

Anderson JD (2004) Introduction to flight. 5th ed. Boston: McGraw-Hill Science Engineering.

Ashrafi ZN, Sedaghat A (2014) Improving the aerodynamic performance of a wing with winglet. Int J Nat Eng. 8(3):52-57

BushnellDM(2003)Aircraftdragreduction–areview.PIMechEngG-JAer.217(1):1-18.https://doi.org/10.1243/095441003763031789

Eguea JP, Catalano FM, Abdalla AM, Santana LD, Venner CH, Silva ALF (2018) Study on a camber adaptive winglet. In: 2018 Applied Aerodynamics Conference. Atlanta: AIAA Aviation Forum. https://doi.org/10.2514/6.2018-3960

Gabor OS, Koreanschi A, Botez RM, Mamou M, Mebarki Y (2016) Numerical simulation and wind tunnel tests investigation and validation of a morphing wing-tip demonstrator aerodynamic performance. Aerosp Sci Technol. 53:136-153. https://doi.org/10.1016/j.ast.2016.03.014

Gabor OS. (2017) Discrete adjoint-based simultaneous analysis and design approach for conceptual aerodynamic optimization. INCAS Bull. 9(3):133-147. https://doi.org/10.13111/2066-8201.2017.9.3.11

Guezguez MS, Botez RM, Mamou M, Mebarki Y (2016) Morphing wing-tip open loop controller and its validation during wind tunnel tests at the IAR-NRC. INCAS Bull 8(3):41-53. https://doi.org/10.13111/2066-8201.2016.8.3.4

Hossain A, Rahman A, Hossen J, Iqbal AKMP, Hasan SK (2011a) Application of fuzzy logic approach for an aircraft model with and without winglet. World Academy of Science, Engineering and Technology 75(3):7-15. https://doi.org/10.1016/j.ast.2010.12.003

Hossain A, Rahman A, Iqbal AKMP, Ariffin M, Mazian M (2011b) Drag analysis of an aircraft wing model with and without bird feather like winglet. World Academy of Science, Engineering and Technology 57:1011-1016.

Houghton EL, Carpenter PW (2003) Aerodynamics for engineering students. Amsterdam: Elsevier Science.

Jones G, Santer M, Debiasi M, Papadakis G (2018) Control of flow separation around an airfoil at low Reynolds numbers using periodic surface morphing. J Fluid Struct. 76:536-557. https://doi.org/10.1016/j.jfluidstructs.2017.11.008

Kammegne MJT, Tondji Y, Botez RM, Grigorie LT, Mamou M, Mébarki Y (2017) New control methodology for a morphing wing demonstrator. P I Mech Eng G-J Aer. 232(8):1479-1494. https://doi.org/10.1177/0954410017699003

Khosravi S, Zingg DW (2014) A numerical optimization study on winglets. In: 15th AIAA/ISSMO Multidisciplinary Analysis and Optimization Conference. Atlanta: Aviation Forum. https://doi.org/10.2514/6.2014-2173

Laybourne RC (1974) Collision between a vulture and an aircraft at an altitude of 37,000 feet. Wilson Bull. 86(4):461-462.

McCormick BW (1967) Aerodynamics of V/STOL flight. Cambridge: Academic Press.

Menter FR (1994) Two-equation eddy-viscosity turbulence models for engineering applications. AIAA J. 32(8):1598-1605. https://doi.org/10.2514/3.12149

Miklosovic DS, Bookey PM (2005) An analytic and experimental investigation of the aerodynamic performance enhancements of multiple winglet configurations. In: Fluids Engineering Division Summer Meeting. Houston: ASME 2005 Fluids Engineering Division Summer Meeting. 1(A-B):259-267. https://doi.org/10.1115/FEDSM2005-77255

Munshi A, Sulaeman E, Omar N, Ali MY (2018) CFD analysis on the effect of winglet cant angle on aerodynamics of ONERA M6 wing. J Adv Res Fluid Mech Therm Sci. 45(1):44-54.

Ning A, Kroo I (2008) Tip extensions, winglets, and c-wings: conceptual design and optimization. In: 26th AIAA Applied Aerodynamics Conference. Honolulu: AIAA Meeting Paper. https://doi.org/10.2514/6.2008-7052

Pratilastiarso J, Nugroho S, Tridianto E, Syifa RI (2018) Experimental study on horizontal axis wind turbine with splitted winglets. IOP Conf Ser Earth Environ Sci. 105(1):12102. https://doi.org/10.1088/1755-1315/105/1/012102

Reddy SR, Sobieczky H, Dulikravic GS, Abdoli A (2016) Multi-element winglets: multi-objective optimization of aerodynamic shapes. J Aircr. 53(4):992-1000. https://doi.org/10.2514/1.C033334

Smith M, Komerath N, Ames R, Wong O, Pearson J (2001) Performance analysis of a wing with multiple winglets. In: 19th AIAA Applied Aerodynamics Conference. Anaheim: AIAA Meeting Paper. https://doi.org/10.2514/6.2001-2407

Tucker V (1993) Gliding birds: reduction of induced drag by wing tip slots between the primary feathers. J Exp Biol. 180(1):285-310.

Weierman J, Jacob JD (2010) Winglet design and optimization for UAVs. In: 28th AIAA Applied Aerodynamics Conference. Chicago: AIAA Meeting Paper. https://doi.org/10.2514/6.2010-4224

Wu R, Soutis C, Zhong S, Filippone A (2017) A morphing aerofoil with highly controllable aerodynamic performance. Aeronaut J. 121(1235):54-72. https://doi.org/10.1017/aer.2016.113